OPERATIONAL PERFORMANCE OF LCLS BEAM INSTRUMENTATION*

H. Loos†, R. Akre, A. Brachmann, R. Coffee, F.-J. Decker, Y. Ding, D. Dowell, S. Edstrom, P. Emma, A. Fisher, J. Frisch, S. Gilevich, G. Hays, Ph. Hering, Z. Huang, R. Iverson, M. Messerschmidt, A. Miahnahri, S. Moeller, H.-D. Nuhn, D. Ratner, J. Rzepiela, T. Smith, P. Stefan, H. Tompkins, J. Turner, J. Welch, W. White, J. Wu, G. Yocky,
SLAC, Menlo Park, CA 94025, USA, R. Bionta, LLNL, Livermore, CA 94550, USA

Abstract

The Linac Coherent Light Source (LCLS) X-ray FEL utilizing the last km of the SLAC linac has been operational since April 2009 and finished its first successful user run last December. The various diagnostics for electron beam properties including beam position monitors, wire scanners, beam profile monitors, and bunch length diagnostics are presented as well as diagnostics for the X-ray beam. The low emittance and ultra-short electron beam required for X-ray FEL operation has implications on the transverse and longitudinal diagnostics. The coherence effects of the beam profile monitors and the challenges of measuring fs long bunches are discussed.

INTRODUCTION

The LCLS facility at the SLAC National Accelerator Laboratory [1] is the first free electron laser operating at angstrom wavelengths. Since 2006 the last 1 km of the SLAC linac has been upgraded to serve as the electron beam source for the FEL and new construction has been added to house the undulator and the X-ray facilities. The first x-ray operation was achieved in April 2009 [2] and a subsequent user run utilized the soft X-ray beam. After commissioning of the hard X-ray beam transport the second user run, later in 2010, will take advantage of the full LCLS capabilities.

Table 1: LCLS accelerator and FEL parameters

	Design	Meas.	Unit
Repetition rate	120	60	Hz
Final energy	13.6	13.6	GeV
Charge	1	0.25	nC
Bunch length	20	7-10	μm
Peak current	3.4	3	kA
Emittance (injector)	1.2	0.4-0.6	μm
Slice emittance (inj.)	1.2	0.4	μm
Emittance (linac end)	1.5	0.5-1.2	μm
X-ray wavelength	1.5	1.5	Å
X-ray pulse energy	1.5	1.5-3.0	mJ
Photons per pulse	2.0	1.0-2.3	10^{12}

The ultra-high brightness electron beam necessary for the operation of an X-ray FEL requires the accurate measurement of a sub-μm emittance and sub 10 μm long electron beam in both transverse and longitudinal coordinates with state of the art diagnostics. The layout of the LCLS is depicted in Fig. 1 with the location of some of the diagnostics devices indicated. The 250 pC electron beam is generated in a laser-driven photocathode RF gun at 6 MeV and subsequently accelerated in four linac sections (L0-L3) to energies of 135 MeV, 250 MeV, 4.3 GeV, and the final energy of 13.6 GeV. After L1 and L2 the bunches are compressed in two chicanes from 750 μm to 40 μm and 10 μm. The beam is then transported through a dog-leg bend magnet system to the 100 m long undulator consisting of 33 segments and dumped in the main beam dump, whereas the generated X-ray beam enters the X-ray diagnostics, transport, and the various experimental areas (not shown). The main parameters of the electron and X-ray beam are listed in Table 1. The design parameters refer to the high charge mode at 1 nC, whereas the measured ones are given for the medium charge operating mode at 250 nC. Recently, a low charge mode with only 20 pC has been explored [3]. The beam in this mode has a slice emittance of 0.14 μm and can be compressed to an estimated final rms bunch length of about 1 μm giving the same peak current and FEL peak power, but a much shorter X-ray pulse $<$10 fs.

Table 2: LCLS Accelerator diagnostics devices

Type	#	Nom. res.	Units
Strip Line BPM	144	5	μm
RF cavity BPM	36	1	μm
Beam current monitor	13	$<$2	%
Phase cavity	5	100	fs
Faraday cup	2	$<$2	%
Wire scanner	17	20	μm
YAG screen	7	15	μm
OTR screen	13	10	μm
Bunch length monitor	2	5	%
Deflecting cavity	2		

A list of all the beam diagnostics devices is given in Table 2 together with their respective highest resolution requirements for each device. In the following sections, the design and operational performance of the various diagnostics for transverse and longitudinal beam parameters, as well as some of the X-ray diagnostics will be discussed.

* Work supported by US DOE contract DE-AC02-76SF00515.
† loos@slac.stanford.edu

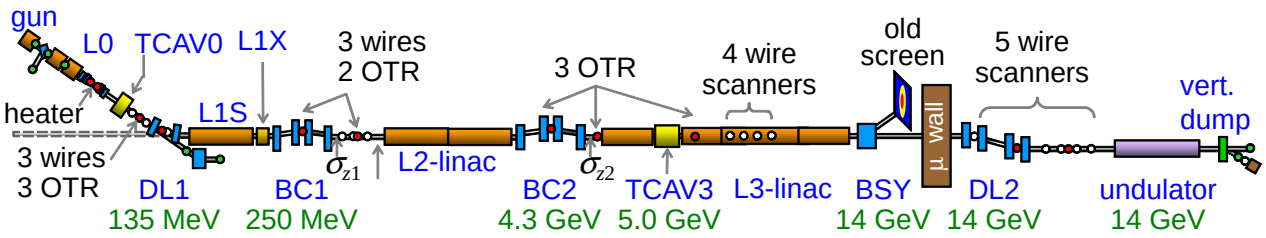

Figure 1: Layout of the LCLS accelerator.

TRANSVERSE DIAGNOSTICS

The main use of the instrumentation for transverse beam diagnostics at LCLS, beam position monitors, wire scanners, and profile monitors is for beam orbit measurement and feedback, and for transverse emittance measurement and optimization. Furthermore, these diagnostics also play an important role for measurements of longitudinal parameters with the transverse defecting cavity.

Beam Position Monitors

Most of the BPMs installed at LCLS are strip line BPMs with more than 80 of them inherited from the SLC linac and more than 60 new ones in the injector and the new transport system to the undulator. The old SLC strip line BPMs were designed to measure beams of nC charge and could not be used for LCLS operation at 20 pC. They have been upgraded over the past year with the same data acquisition electronics as for the new LCLS BPMs and have all been integrated into the EPICS control system. All strip line BPMs are continuously calibrated between beam triggers by sending 4 test pulses in each of the electrodes. Two attenuators are used to scale the signals to the charge levels at different operating modes.

A beam synchronous acquisition system enables the pulse by pulse measurement of all BPMs together with other control system parameters for up to 2800 bunches at all LCLS beam rates from single shot to 120 Hz. Besides providing shot by shot beam orbits, this acquisition system can also be used to measure the BPM resolution as shown in Fig. 2. In a model independent analysis (MIA) [4] a singular value decomposition of the matrix of measured beam orbits yields an orthogonal basis of all the different jitter and noise contributions. The strongest singular values represent correlated beam motion and the figure shows the remaining rms noise from 500 orbits after subtracting the effect of the largest 10 values. At 250 pC the average noise of the strip line BPMs is 3 μm which is well below the beam size of several 10s of μm of the LCLS electron beam. For the low charge 20 pC beam the BPM signal becomes weak and the noise rises to 25 μm rms which at many locations can be comparable to the rms beam size for this low charge.

For a stable FEL operation the beam orbit within the 100 m long undulator needs to be straight within only a few μm over a distance of several of the 33 segments. This requirement of sub-μm resolution and offset stability could be met with RF cavity BPMs [5] located at the end of each girder which supports one of the 3 m long undulator segments and a quadrupole besides the BPM. The BPMs [6] consist of two cavities, one degenerate dipole mode cavity and one reference cavity for signal normalization with both operating at 11.4 GHz. The signal is then down-converted to 40 MHz IF and analyzed in a 16 bit VME digitizer. In contrast to the strip line BPMs the calibration of the RF BPMs has to be done using signals from the electron beam itself. This can be done in two different ways. A slow method with high precision is to move the girder which supports the BPM and the respective undulator segment by known amounts and observe the change in the beam position measured by the BPM. A faster way is to use a corrector magnet to introduce an orbit oscillation upstream of the undulator whose magnitude is measured with the upstream strip line BPMs and then measuring the response of the cavity BPMs. The resolution can again be obtained

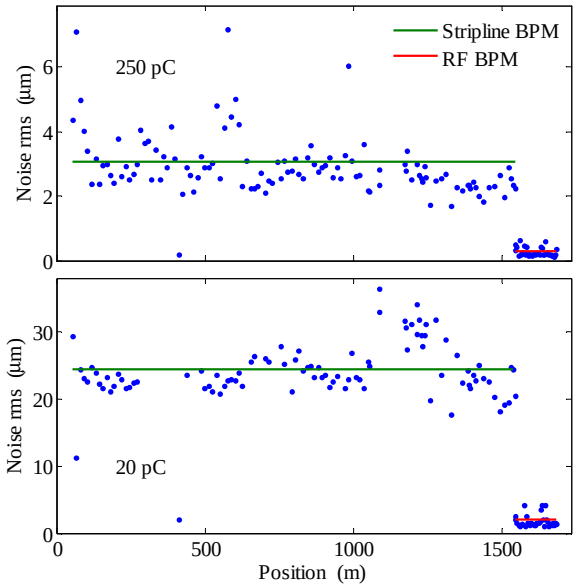

Figure 2: Measured BPM noise level along the accelerator. The top part is at 250 pC with an average noise of 3 μm for the strip line (green) and 300 nm for the RF BPMs (red), the bottom one is at 20 pC with 25 and 2 μm, respectively.

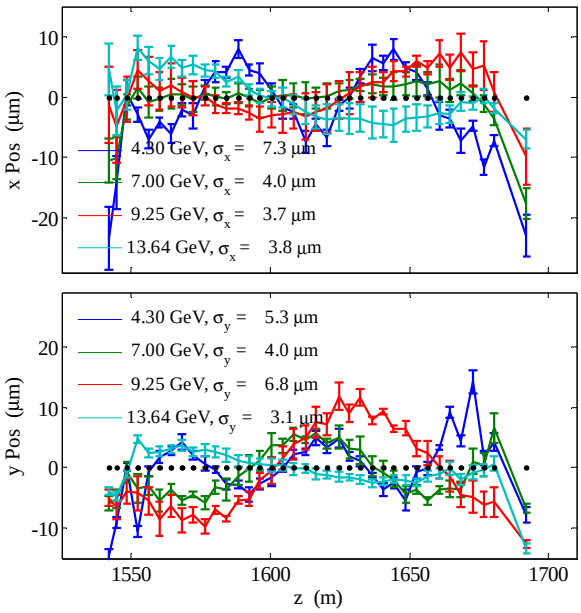

Figure 3: Beam orbit measured with RF BPMs and averaged over 50 shots in the undulator at 4 different energies after applying beam based alignment. The orbit rms deviation σ includes incoming betatron oscillation due to upstream beam jitter.

from signal correlations between BPMs and is also shown in Fig. 2. The average noise level at 250 pC of 300 nm is well below the requirement and most of the BPMs are even around 200 nm. The noise level grows to 2 μm at 20 pC.

The effect of the sub-μm RF BPM resolution can be seen in the results of the beam-based alignment (BBA) procedure for the undulator segments. The FODO lattice within the undulator is designed to be operated at the same field within the nominal energy range from 4.3 to 13.64 GeV of the LCLS electron beam. A measurement of the beam orbit at several energies spanning this range can be used to find both the deviations of the BPM positions and of the absolute beam orbit from a straight line. The position of the quadrupoles and the BPM offsets can then be corrected to generate a dispersion free beam orbit at the BPM locations [7]. Figure 3 shows beam orbits averaged over 50 beam pulses for 4 different energies after applying several iterations of the correction procedure. The remaining rms orbit deviation is only a few μm and results mostly from incoming beam position jitter.

Wire Scanners

Wire scanners are used at various locations in the accelerator to provide measurements of transverse and longitudinal beam profiles in a less interceptive way than view screens because the beam hits the wire only for a few pulses. A wire card holding three wires in vertical, horizontal, and one in 45° direction is moved through the beam at an angle of 45° so that each of the horizonal, vertical, and 45° projection can be measured. The tungsten wires have diameters of 20 - 40 μm which are matched to the respective beam size at the wire scanner location. This sets a resolution limit of 5 - 10 μm based on the finite thickness which can be subtracted from the beam size measurements in the analysis software. The wires are moved by stepper motors and transverse vibrations of the wire card of 10s of μm which were observed at the beginning of the LCLS commissioning could be significantly reduced by either the installation of gear reducers or the use of microstepping for the motors. The bremsstrahlung generated at the wires is detected with fast ion chambers, with PMTs detecting Cherenkov radiation from secondary electrons, or with PMTs looking at the light from plastic scintillator fibers strapped along the beam pipe.

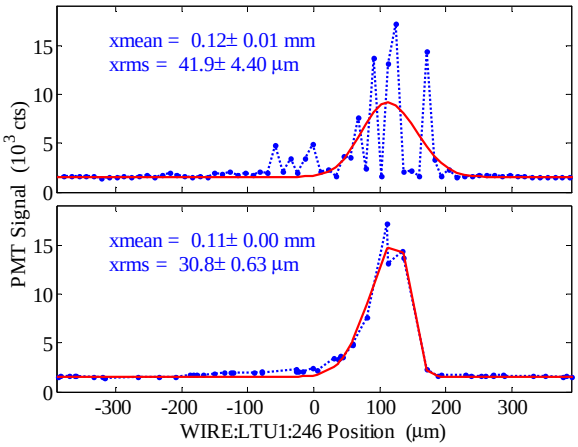

Figure 4: Beam jitter correction for wire scan data. The top part shows the PMT signal vs. the raw wire position with an rms beam size of 42 μm. In the bottom part the wire position is corrected shot by shot and the rms beam size reduces to 31 μm.

Essential for a high resolution beam size measurement is a correction of the effect of the transverse beam position jitter. This requires the synchronous measurement of the beam position at several nearby BPMs together with the PMT signal and the wire position for each bunch. A beam orbit fit then determines the distance of the beam to the wire for each bunch. This correction is particularly important in an energy spread or bunch length measurement where the transverse jitter can exceed the beam size. The effect of the jitter correction is shown in Fig. 4 for the wire scanner in a dispersive location in the DL2. The beam jitter correction also enables precise beam size measurements for emittance measurement and beta-matching of the lattice as shown in Fig. 5.

When the transverse beam jitter or a deliberate transverse motion of the beam exceeds the beam size, this can be used to measure beam profiles without scanning the wire. The profile is then sampled by the beam jitter alone. One application is to measure beam parameters in a pulse

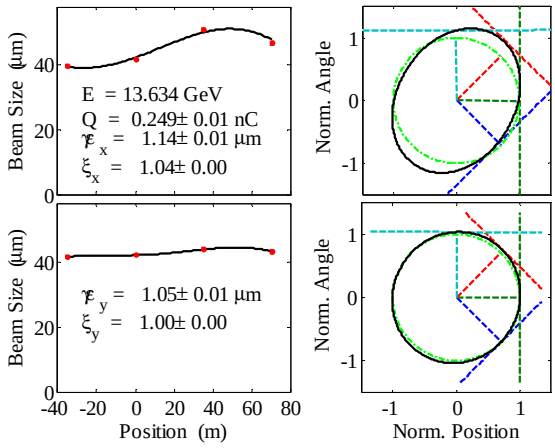

Figure 5: Emittance measurement upstream of the undulator using 4 wire scanners with 45° phase advance between them. The left panels show the measured beam sizes in the horizontal and vertical plane, and the right panels the respective normalized phase space ellipse. The dashed lines indicate the projection angle for each measurement.

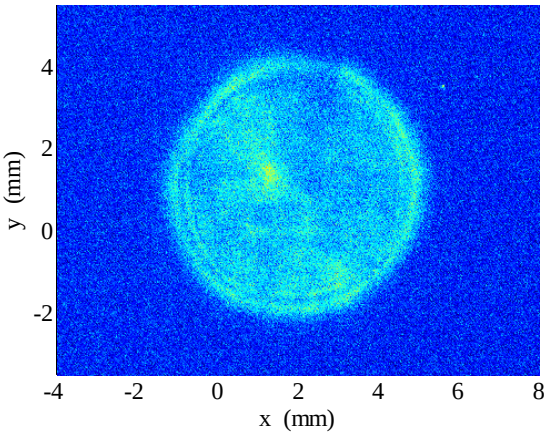

Figure 6: Electron beam distribution at 15 pC charge on a YAG screen downstream of the gun showing the electron emission pattern from the cathode.

stealing mode. The wire is parked at a location near the beam and a small fraction of the bunches at 1 Hz is transversely kicked to intercept the wire while the majority of the bunches is still delivered to the FEL user. An example of this almost non-intercepting diagnostic method is the pulse stealing bunch length measurement discussed later.

Beam Profile Monitors

The beam profile monitors enable the measurement of single shot transverse beam distributions throughout the accelerator and are mainly used for emittance, energy spread and bunch length measurements. In the low energy part of the machine at energies below 135 MeV they consist of 100 μm thin YAG:Ce crystals perpendicular to the beam and a 1 mm thick mirror behind it for viewing at 90 degrees. At 130 MeV and above, 1 μm thin aluminum foils are employed as optical transition radiation (OTR) screens at 45 degrees to the beam. Beam images from both targets are obtained with a 50 mm focus telecentric lens and a mega-pixel CCD camera with an effective pixel resolution as low as 10 μm/pixel. The depth of focus of about 1 mm provides an equally wide stripe of adequate image quality for the 45 degree OTR foils and the geometry is chosen to match the stripe direction with the dispersion direction or the streak direction of the deflecting cavity. The small resolution is sufficient to measure beam sizes as small as 25 μm whereas the large number of pixels provides a field of view necessary to measure a dispersed beam or the beam deflected with the deflecting cavity. The 12 bit ADC of the cameras equate to a S/N ratio of 1000. This gives a dynamic range of larger than 10^5 together with the two insertable neutral density filters having an attenuation of up to 1000.

The YAG screens are mainly used in the gun area at a beam energy of 6 MeV where the photon yield for OTR is too low and at higher energy in the injector where the beam size is large and saturation is not a concern. They are used in the gun area for their high sensitivity to measure the electron beam emission pattern from the photo-cathode at a charge of only a few pC and in the injector spectrometer at 135 MeV where the beam can be streaked with a deflecting cavity to observe the longitudinal phase space. Figure 6 shows the beam spot on a YAG screen right after the gun with the gun solenoid magnet set to image the electron distribution generated on the cathode by the laser onto the downstream YAG screen. A low charge of 15 pC is necessary to avoid space charge distortions.

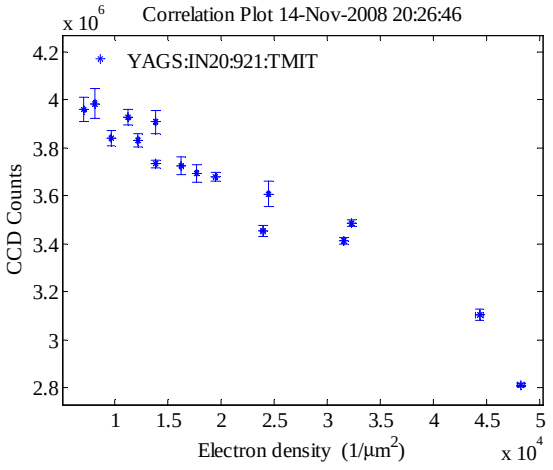

Figure 7: Image intensity of a YAG screen as a function of electron density on the crystal. The density was varied by scanning an upstream quadrupole.

For higher charges quantitative beam size measurements with a YAG screen are limited by saturation effects in the

YAG:Ce crystals. Figure 7 shows a measurement of the total CCD counts on a YAG screen in the injector spectrometer line at 135 MeV. An upstream quadrupole magnet was scanned to vary the beam size and the plot shows the integrated image intensity as a function of the calculated electron density. Saturation occurs at densities higher than 15000 $e^-/\mu m^2$ which corresponds to a rms beam size of 130 μm at 250 pC. This makes YAG screens unsuitable for most locations in the accelerator where the beam size can be significantly smaller.

The emission of optical transition radiation has about a factor 1000 lower quantum efficiency compared to scintillator screens, but it does not show saturation effects and the resolution is not limited from the finite crystal thickness. The beam going through a 1 μm foil can still be transported through the remainder of the accelerator with negligible beam loss. OTR screens were therefore installed in the injector and the BC1, BC2, and DL2 areas to measure the projected and time resolved (slice) emittance, as well as energy spread and bunch length. In the undulator for the injector laser heater two OTR foils are used to transversely overlap the electron beam with an 800 nm wavelength laser beam [8].

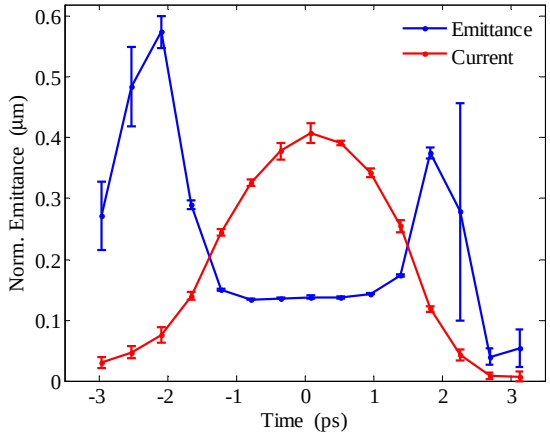

Figure 8: Measurement of the horizontal slice emittance in the injector at 20 pC. The normalized emittance in the core slices of the beam is 0.14 μm.

Originally specified to diagnose beams of a charge between 250 pC and 1 nC, the lens and camera system proved to be able to measure the time resolved beam size of a 20 pC beam in the injector with a slice charge as low as 2 pC. Figure 8 shows the result of such a measurement where the transverse deflector cavity in the injector was used to vertically deflect the electron beam and with a quadrupole scan the horizontal beam size and slice emittance could be obtained. At 20 pC the core of the beam has a normalized emittance of only 0.14 μm. Figure 9 shows the beam size as a function of the quadrupole strength for slice number 6 near the center of the beam with the beam size as small as 25 μm.

The OTR screens proved very reliable in the injector part

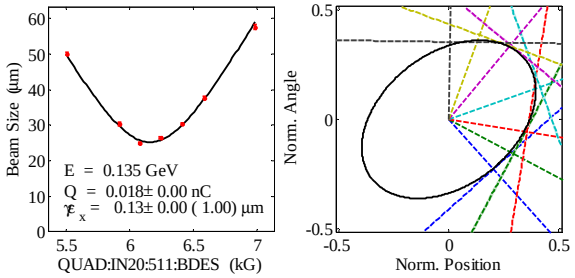

Figure 9: Beam size and normalized phase space of slice number 6 from the measurement shown in the previous figure.

of the LCLS, however, the unexpected observation of coherent effects in the optical transition radiation (COTR) in the accelerator downstream of the injector made these diagnostics much less useful. The coherent effects originate from a longitudinal structure in the beam at optical wavelengths and are manifest in a non-linear relation between charge and OTR intensity and therefore the transverse OTR distribution is not proportional to the charge distribution. At bunch lengths of a few ps to 100s of fs this is due to longitudinal space charge forces modulating the energy distribution of the beam. After traveling through a bend magnet system with a non-zero R_{56} matrix element, the modulation appears in the time domain and the bunch emits coherent radiation. The effect on the beam size measurement can be seen in Fig. 10. The beam size is measured downstream of the 35° DL1 bend system with the strength of the dispersion correction quadrupole inside the dog-leg varied. The expected small change of a few % in beam size from the varied quadrupole strength is shown as a red line. The measured size of the OTR distribution drops by a factor of 2 around the optimum quadrupole strength of 10.8 kG where the dispersion is fully canceled. This change in apparent beam size is accompanied by a factor 3 increase in the OTR intensity (not shown).

More dramatic effects occur when the LCLS beam is compressed to bunch lengths in the range of 10s of μm to a few μm rms. Then the bunch length is only a factor 10 longer than the visible OTR wavelengths and a significant fraction of the beam can radiate coherently [9]. The light intensity can increase by up to 5 orders of magnitude and the transverse OTR distribution becomes fractured or ring-shaped.

A possible mitigation scheme is to use a YAG crystal instead of the OTR foil at locations with a large beam size. The YAG crystal surface will still emit OTR with about a factor 3 less than from a foil, but the YAG fluorescence is about 3 orders of magnitude larger than the incoherent OTR. This ratio can be further enhanced with a narrow band pass filter at the YAG peak emission wavelength of 525 nm and a few degree tilt of the crystal to prevent the highly collimated COTR light from entering the camera optics. Such a setup was recently installed in the LCLS

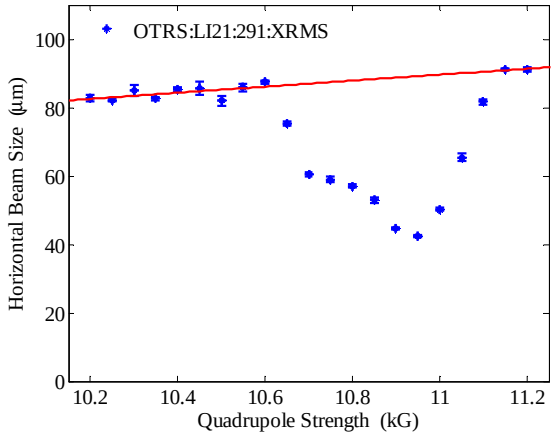

Figure 10: Measured OTR distribution rms size downstream of DL1 with the dispersion correction magnet in DL1 varied. Shown in red is a smooth line indicating the expected small change in true beam size from the varied quadrupole.

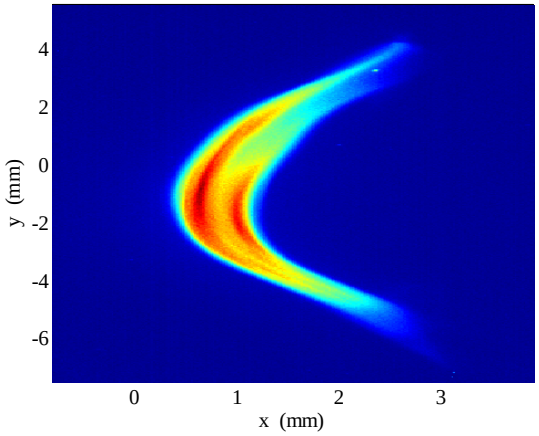

Figure 11: Longitudinal phase space on the YAG screen in the injector spectrometer. The horizontal axis is dispersed showing energy spread whereas the vertical axis is streaked by the deflecting cavity to show the temporal distribution. The image clearly shows the double peak structure in the energy distribution due to the laser heater interaction.

main dump line to replace the existing OTR screen and its performance is currently studied. The increased beam loss due to the 100 μm thick crystal is not a high concern at this location, but how to replace the OTR screens at other locations in the linac and especially upstream of the radiation sensitive undulator is an open question.

LONGITUDINAL DIAGNOSTICS

A precise measurement of both the ps long bunch length in the injector and the ultra-short bunch lengths of the compressed beam with lengths of only a few μm is essential to obtain the kA peak currents required for operation of the FEL. The absolute bunch length measurement is done with transverse deflector cavities, whereas a relative measurement needed for the longitudinal feedback uses a measurement of integrated far infrared coherent radiation from the bunches.

Transverse Deflecting Cavities

Two transverse deflecting cavities [10] are installed in the LCLS. The first one in the injector with 50 cm length is used to measure the initial bunch length and slice emittance of the beam and is operated at about 1 MV field. The phase of the cavity is set to one of the zero-crossings of the field so that the head and tail of the bunch are kicked vertically in opposite directions. This maps the longitudinal distribution onto the vertical axis and the mapping can be calibrated by changing the phase of the cavity away from the zero-crossing to observe the vertical motion of the beam centroid. The use of the deflecting cavity for time resolved emittance measurement was discussed earlier (see Fig. 8).

A measurement of the longitudinal phase space is shown in Fig. 11 with the beam observed on a YAG screen in the injector spectrometer. The horizontal axis represents the energy spread and the vertical axis the temporal distribution. The double horn structure in the energy distribution shows the effect of the laser heater to increase the uncorrelated energy spread of the beam from 3 to 10s of keV, depending on the energy of the laser heater [8].

The second, 2.44 m long transverse deflecting cavity is located in the L3 linac after the second bunch compressor and operates at 15 MV field to accommodate the much shorter bunch length there. An off-axis OTR screen located downstream of the deflecting cavity at 90° degree phase advance to map the vertical kick of the cavity onto vertical displacement was originally intended to measure the streaked beam profile with pulses steered onto the screen with a fast horizontal kicker magnet. The strong COTR emission from the ultra short beam prevented reliable beam profiles and instead a lower resolution legacy phosphor screen in the beam switch yard of the SLC was used [11]. This screen is not in the LCLS beam line and requires a special beam setup, therefore more recently, a bunch length measurement was set up to use one of the 4 wire scanners in the L3 linac downstream of the deflecting cavity.

The deflecting cavity calibration factor for the wire scanner with the proper phase advance is about 2 μm/fs and the 50 fs timing jitter between the electron bunches and the cavity phase translates into 100 μm rms vertical orbit jitter at the wire scanner. This is twice the beam size and a precise jitter correction is essential. The pulse stealing mode for the wire scanners described above can be applied with the deflecting cavity triggered at 1 Hz while the pulses used for the FEL run at a higher rate of 10 to presently 60 Hz. During the 99 pulses acquired the wire is moved to 3 different off-axis positions with about 0.5 mm spacing to capture the entire beam profile. The measured PMT signals vs. the

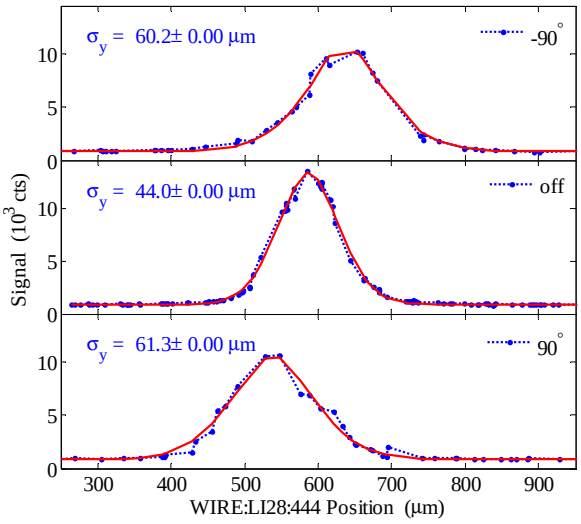

Figure 12: Beam profiles for bunch length measurement in 1 Hz pulse stealing mode. The top and bottom part show the profile with the deflecting cavity at $\pm 90°$ and the wire placed at three positions. The middle part shows the intrinsic vertical beam size measured with the wire in 13 different positions. The wire locations are corrected for beam jitter.

relative position between wire and beam is shown in Fig. 12 at 250 pC for the two zero-crossing phases $-90°$ and $+90°$ and for the case with the cavity off. In this case the transverse jitter is only a small fraction of the beam size and the wire was placed at 13 different positions to obtain a full beam profile. The beam sizes are about 60 μm with, and 44 μm without the cavity on.

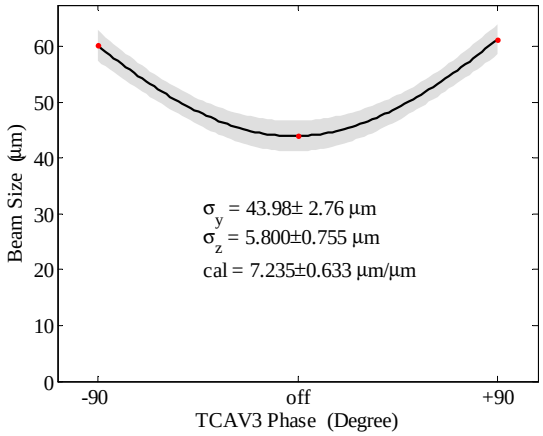

Figure 13: Bunch length measurement with wire scan in pulse stealing mode with data points from the previous figure. The data point at 0○ is with the cavity off. The bunch length is 5.8 μm.

To obtain the bunch length the intrinsic transverse beam size has to be subtracted in quadrature from the streaked beam size and then the calibration factor needs to be applied. The result is shown in Fig. 13 with a rms bunch length of 6 μm which represents a slightly more compressed beam than the nominal 7 μm long bunch. The error on the measured length is less than 1 μm. In pulse stealing mode this measurement takes only about 5 min and can be run parasitically to the user operation to monitor the peak current with an absolute measurement.

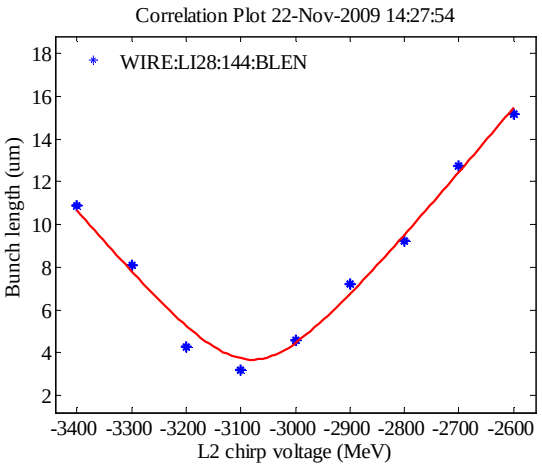

Figure 14: Scan of the rms bunch length vs. chirp voltage in the L2 linac. The normal operating point is around -2900 MeV with an under-compressed bunch length of 7 μm. The shortest bunch length is 3.5 μm. Shown in red is a fit to the measured bunch length assuming linear compression.

The full range of bunch lengths can be measured when the phase or equivalently the chirp voltage of the L2 linac upstream of the second bunch compressor is varied. The result of this scan using the normal scan mode of the wires at full beam rate is shown in Fig. 14 with an under-compressed beam to the right and an over-compressed beam to the left. At full compression the beam is as short as 3.5 μm rms.

For the 20 pC low charge operation sub-μm bunch lengths have been predicted by simulations [3]. With a smaller intrinsic beam size at low charge a measurement of much shorter bunch lengths than 3 μm rms should be possible. However, this has not been successful yet because the necessary jitter correction is insufficient at low charge. The BPM noise of 25 μm is of the order of the transverse beam size and the error of the size measurement is larger than the expected increase in beam size due to the streak from the deflecting cavity. A cavity operating at the X-band frequency 11.4 GHz and more than twice the voltage is in development to be placed downstream of the undulator. Such a system could have 10 times the resolution compared to the present system after BC2 and should be able to measure sub-μm bunch lengths.

Relative Bunch Length Monitors

The longitudinal feedback system for the LCLS requires a single shot non-intrusive measurement of the bunch length which does not have to be absolute. This is accomplished with relative bunch length monitors [12] using the coherent edge radiation [13] emitted from the exit edge of the last dipole magnet in each bunch compressor chicane. The radiation is emitted in a cone and reflected off the beam axis by an annular mirror with a 15 mm diameter aperture to pass the electron beam undisturbed. The radiation is imaged with off-axis paraboloidal mirrors onto pyroelectric detectors to integrate the far infrared spectral range which is strongly correlated to the bunch length. A shorter bunch emits a radiation spectrum which extends further to shorter wavelengths, thus increasing the integrated intensity. Insertable low and high pass filters can be used to optimize the wavelength range for the detector. Two bunch length monitors are installed, one after each bunch compressor. The wavelength range most sensitive to the bunch length σ_z extends from $2\pi\sigma_z$ to longer wavelengths. For the monitor after BC2 a diffusive low pass filter with 100 μm cutoff wavelength rejects the near IR radiation emitted from micro-structure within the bunch which is unrelated to the bunch length.

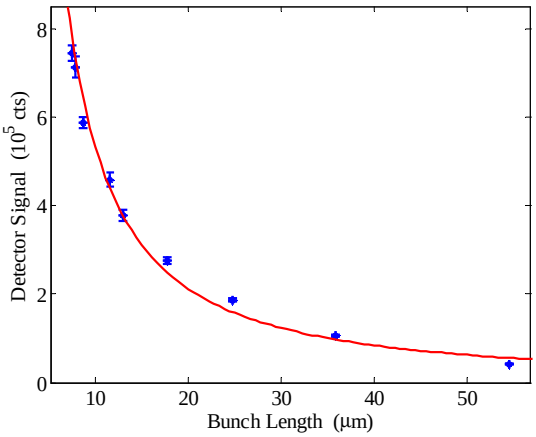

Figure 15: Calibration of the relative bunch length monitor after BC2 with an absolute measurement using the deflector cavity and a wire scanner. The red line is a fit to the data using an inverse 4/3 power law of the bunch length.

Figure 15 shows the raw signal from the pyroelectric detector after BC2 as a function of the bunch length measured with the deflecting cavity and a wire scanner in L3. The red line is a fit of the signal to the bunch length assuming a signal dependency to the inverse 4/3 power of the bunch length and a quadratic dependency to the bunch charge. The fit parameter is then used in the control system to calculate a bunch length from the shot by shot signal and convert it into a peak current value assuming a parabolic charge distribution [14]. This enables a peak current set point for the feedback system.

X-RAY DIAGNOSTICS

The diagnostics for the x-ray beam generated in the LCLS undulator is mainly located in the front end enclosure (FEE) downstream of the main dump and before the user experiments. It comprises of adjustable beam collimators, a solid and a gas attenuator system for hard and soft x-ray energies respectively, two gas detectors, a direct imager, a fixed photon energy monochromator system, and a total energy monitor. A diagnostic with a electron beam type YAG screen was installed in the main dump area in the photon beam line after the dump bend magnet system prior to the LCLS start-up in early 2009 as a preliminary X-ray diagnostics before the systems in the FEE became available.

Energy Measurement

An absolute measurement of the X-ray photon energy is done by measuring the loss in energy of the electrons during the lasing interaction in the undulator. The electron beam energy loss is determined for each shot by comparing the beam energy in the main dump line with the beam energy in DL2 upstream of the undulator as measured from BPM positions. The determination of the energy loss has to take into account the losses due to wake fields in the narrow undulator vacuum chamber as well as losses due to spontaneous radiation emission. This is done by comparing the electron beam energy loss with the electron beam on the undulator beam axis with the energy loss when the beam is kicked on an off-axis orbit which suppresses lasing, but does not influence the other two kinds of energy loss.

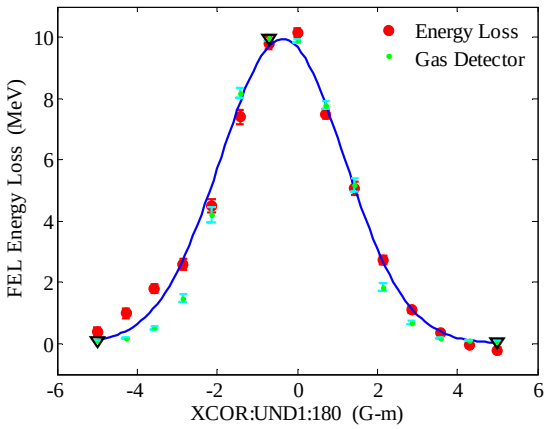

Figure 16: FEL pulse energy determination by electron beam loss and gas detector measurements.

A scan of the beam energy difference between various orbits in the undulator is shown in Fig. 16 at 4.3 GeV electron beam energy and 820 keV photon energy with the beam energy of the most disturbed orbit as zero-reference. The maximum energy loss of 10 MeV per electron at the peak corresponds to 2.5 mJ X-ray pulse energy for a bunch

charge of 250 pC. This invasive measurement can then be used to calibrate or compare the X-ray energy measurements in the FEE.

A non-intrusive single shot measurement is provided by the two gas detectors [15] in the gas attenuator system in the FEE. A section of the photon transport vacuum line can be brought to a pressure of up to 20 Torr of nitrogen gas with a differential pumping system. At the location of the gas detectors between the pumping stations the pressure is between 0.1 and 2 Torr, depending on the X-ray wavelength. The nitrogen gas being hit by the X-rays emits Auger electrons which are trapped by a magnetic field in the vacuum chamber to generate secondary electrons which in turn cause light emission in the UV from the nitrogen gas. The light is then detected by PMTs or avalanche photodiodes. The signal from the gas detectors depends strongly on the X-ray wavelength and intensity.

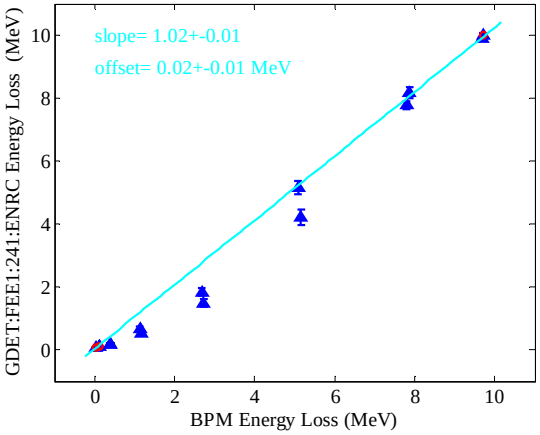

Figure 17: Gas detector calibration from energy loss scan.

Figure 17 shows the calibrated gas detector signal as a function of the energy loss as measured with the electron beam loss shown in the previous figure. This kind of calibration is done routinely whenever the photon energy is changed and takes only about 30 s.

Transverse Diagnostics

The measurement of X-ray position and beam size uses the same kind of YAG:Ce crystals used for electron beam diagnostics. The two different screens mainly used are the one in the quick-change diagnostic chamber in the main dump area about 50 m downstream of the undulator and the screen on a target ladder in the direct imager downstream of the X-ray attenuators and about 80 m past the undulator. Figure 18 shows the YAG screen in the dump area with the FEL operated at 13.64 GeV. Besides the main X-ray spot in the screen center, the rectangular shaped background of spontaneous emission shadowed by the undulator vacuum chamber and the circular ring pattern of visible light emitted from the exit edge of the first dump dipole magnet is visible. A vertical diffraction pattern from a 20 μm thick carbon wire inserted into the X-ray beam at the last undulator segment is also present in the image and can be used to estimate the transverse coherence of the X-ray beam.

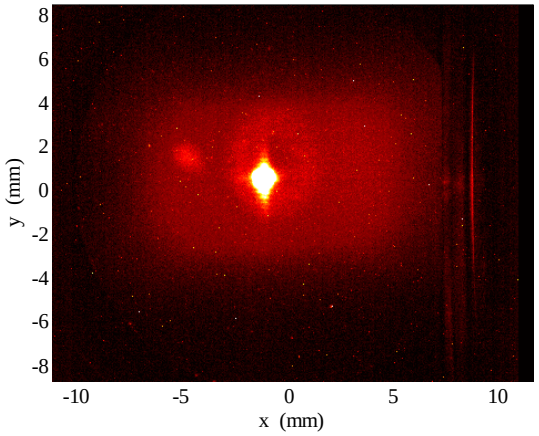

Figure 18: Image from the YAG screen in the photon beam line after the main dump at an electron beam energy of 13.6 GeV. The image shows the X-ray pulse as well as the background from spontaneous radiation and the visible ring pattern of edge radiation from the first dump bend magnet.

The X-ray beam image at 2 keV photon beam energy is shown in Fig. 19 for the narrow field of view (NFOV) direct imager with a 1 mm thick YAG crystal inserted. The camera is a high dynamic range cooled CCD with a 16 bit digitizer and a 512×512 pixel array. Besides beam size measurements, both screens are also used to measure the X-ray pulse energy as a function of undulator length to determine the gain length of the FEL. In contrast to the gas detector measurement the sensitivity of the screens can quickly be changed with light attenuators and an absolute energy measurement is not necessary.

SUMMARY

The diagnostics implemented for the LCLS electron beam has made it possible to measure and achieve all the transverse and longitudinal beam parameters required for a successful operation of the FEL. All the diagnostics are well integrated into the EPICS control system and high level Matlab applications provide automated measurement procedures and displays for all beam parameters. The unexpected appearance of COTR compromising the beam profile measurement of the compressed bunches could be offset by using existing wire scanners and installing additional ones in DL2 and the main dump. Time resolved measurements of emittance and energy spread however require the acquisition of 2-D distributions and an adequate substitute or COTR mitigation for the OTR screens has not been found yet. New diagnostics are also necessary to measure the sub-μm long bunches in the low charge operating mode and various schemes are being discussed. The commissioning of the soft X-ray user beam line will provide a single

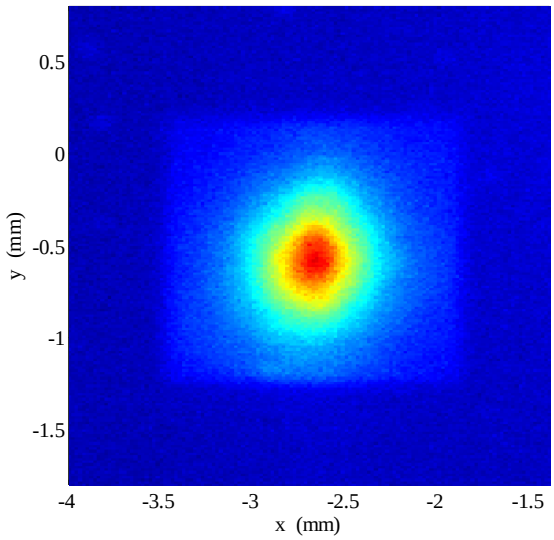

Figure 19: Image from a YAG screen in the direct imager showing the FEL pulse and the spontaneous radiation clipped by upstream collimator jaws.

shot X-ray spectrum measurement which will complement the X-ray monochromator in the FEE operating at the fixed photon energy of 8.3 keV. Additional instrumentation for energy measurement with a thermo-acoustic sensor will be added to the quick-change diagnostic chamber in the main dump area. One remaining issue for future diagnostics development is the absolute measurement of the X-ray pulse length.

REFERENCES

[1] J. Arthur, *et al.*, Linac Coherent Light Source (LCLS) conceptual design report, SLAC-R-593, SLAC (2002).

[2] P. Emma, Proceedings of PAC 2009, Vancouver, BC, May 2009, p. TH3PBI01 (2009).

[3] Y. Ding, *et al.*, Phys. Rev. Lett. 102 (2009) 254801.

[4] J. Irwin, *et al.*, Phys. Rev. Lett. 88 (1999) 1684.

[5] S. Smith, *et al.*, Proceedings of PAC 2009, Vancouver, BC, May 2009, p. TU3GRC05 (2009).

[6] R. M. Lill, *et al.*, Proceedings of PAC 2007, Albuquerque, NM, June 2007, p. FRPMN111 (2007).

[7] P. Emma, *et al.*, Nucl. Instr. and Meth. A 429 (1999) 407.

[8] Z. Huang, *et al.*, Phys. Rev. ST Accel. Beams 13 (2010) 020703.

[9] H. Loos, *et al.*, Proceedings of FEL 2008, Gyeongju, Korea, Aug. 2008, p. THBAU01 (2008).

[10] O. H. Altenmueller, R. R. Larsen, G. A. Loew, Rev. Sci. Instrum. 35 (1964) 438.

[11] R. Akre, *et al.*, Phys. Rev. ST Accel. Beams 11 (2008) 030703.

[12] H. Loos, *et al.*, Proceedings of PAC 2007, Albuquerque, NM, June 2007, p. FRPMS071 (2007).

[13] R.A. Bosch, Rev. Sci. Instrum. 73 (2002) 1423.

[14] J. Wu, *et al.*, Proceedings of FEL 2008, Gyeongju, Korea, Aug. 2008, p. MOPPH052 (2008).

[15] S. P. Hau-Riege, *et al.*, J. Appl. Phys. 103 (2008) 053306.